Two-photon luminescence of gold nanorods: applications to single-particle tracking and spectroscopy

Carozza, S.

Chapter 4

Functionalization and nuclear targeting of single gold nanorods in live cells

Functionalization of gold nanorods is a necessary step for targeted delivery and for their use as labels to follow specific molecules in cells. Here, we functionalized gold nanorods with nuclear localization signal peptides and delivered them in live HeLa cells by single-cell microinjection. We used a two-photon multifocal scanning microscope to acquire 3D images of gold nanorods in cells. The efficiency of single-cell microinjection showed some variability between experiments and influenced the nuclear targeting results. Nevertheless, we observed nuclear localization of gold nanorods only when functionalized with the peptide. The nuclear targenting efficiency was around 15%, probably limited by the size of the particles. We noticed clearance of gold nanorods from the cytoplasm over time, both functionalized and not functionalized. The mobility of the nanorods did not depend on their functionalization. Overall, these experiments show that functionalization of gold nanorods with nuclear localization signal can be used for nuclear targeting, but only with a small yield.

Single-Particle Tracking of Gold Nanorods in Live Cells, S.Carozza, V. Keizer, A. Boyle, A. Kros, M. Schaaf, J. van Noort. (in preparation partially based on this chapter).

4.1 Introduction

Gold nanorods (GNRs) have a high potential as labels for single-molecule imaging in live cells, thanks to their brightness, stability and excitation with low energy radiation that minimizes autofluorescence and photodamage in the cells. For such an application, they can be functionalized to bind to specific proteins, organelles or cells.

Next to single-particle imaging, GNRs have been used to selectively kill cancer cells, through gene-therapy [1] or photothermal therapy, due to their capability to enhance electromagnetic fields and generate heat upon irradiation with nearIR light [2]. Applications in cancer therapy usually target nanoparticles to the nucleus, where the therapeutic effect is maximum [2]. Though nuclear targeting has been well established for these practices, its mechanism has, to the best of our knowledge, not been studied at the single particle level, which will bring insights in the efficiency of delivery and is a prerequisite for single-particle tracking applications of GNRs.

In this study, we tested the functionalization of GNRs with a nuclear localization signal (NLS), a peptide that signals transport of molecules from the cytoplasm to the nucleus [3]. Nuclear localization of GNRs is the evidence of a successful functionalization with NLS and subsequent integration in the cellular transport pathway. The efficiency of nuclear delivery depends on the size of the nanoparticles. Due to the complex structure of the nuclear pores, small particles can diffuse passively through the membrane, but an active transport mechanism is necessary for larger particles [4]. Literature reports passive diffusion to the nucleus for particles with a size up to 10 nm [4, 5].

Active transport in the nucleus is typically achieved through conjugation with nuclear localization peptides [6], but other conjugations can also be used [7]. Successful nuclear targeting of particles with sizes up to 40 nm, functionalized with NLS, has been reported in several studies [8–13].

The GNRs we use for our experiments are approximately 53 nm x 20 nm. Previously, we observed no passive translocation of 40 nm x 10 nm GNRs in the nucleus without NLS functionalization (see Chapter 3). In the current study, we quantified the uptake of NLS-GNRs in the nucleus of live HeLa cells over time, as compared to GNRs without NLS sequence. Although there are many recent reports on the use of nanoparticles in cells, few quantify their uptake over time. To be able

to enter the nucleus when equipped with NLS, GNRs must be free to diffuse in cell and not trapped inside vesicles. We delivered GNRs in cells through single-cell microinjection, to avoid the uptake into vesicles which is common to passive delivery methods such as incubation. In addition, we characterized the reproducibility of the injection method. To localize GNRs in cells we used images acquired with a two-photon multifocal scanning microscope [14]. This setup acquires 3D movies of cells which can subsequently be processed to yield GNR localization with nm accuracy. We studied the mobility of GNRs functionalized with NLS and control GNRs in the cytoplasm, and compared the results with the ones obtained previously with non-functionalized GNRs.

4.2 Materials and methods

NLS synthesis

The NLS peptide was synthesized with a peptide synthesizer (Liberty 1, CEM), on a Rink-amide resin using HCTU (1H-Benzotriazolium 1-[bis(dimethylamino)methylene] -5chloro-,hexafluorophosphate (1-), 3-oxide) as a coupling agent and DIPEA (Diisopropylethylamine) as base. After synthesis, the peptide was acetylated at the N-terminus using a solution of acetic anhydride (5%) and pyridine (6%) in DMF (Dimethylformamide). After one hour, the peptide was cleaved using a solution of 95% trifluoroacetic acid (TFA), 2.5% water and 2.5% triisopropylsilane (TIPS). After one hour, the peptide was precipitated into ice-cold diethyl-ether, the precipitate collected by centrifugation, redissolved in water and freeze-dried to obtain a powder. The peptide was then purified by reverse-phase HPLC (high-performance liquid chromatography) over 30 minutes.

GNR preparation and functionalization

GNRs were produced by seed-mediated synthesis, as described in [15]. GNRs were then PEGylated, by addition to the solution of Polyethylene-Glycol 5000 in excess, to reduce toxicity of the particles [16]. PEG-GNRs were then functionalized with a sulfo-SMCC molecule, used as a cross-linker to the NLS. Conjugation with sulfo-SMCC was obtained by addition of 0.1 mg sulfo-SMCC solution to 5 ml 0.1 nM of PEG-GNR solution. The procedure was optimized to cover the entire surface of

the PEG-GNR with sulfo-SMCC. The solution was then left to stir for 30 minutes, centrifuged and the supernatant sulfo-SMCC was removed before resuspension of the solution in Phosphate-Buffered Saline (PBS).

For conjugation of NLS to GNRs, 1 ml of solution containing 1 mg of the NLS peptide was added to 4 ml of sulfo-SMCC-GNRs dissolved in PBS. The solution was then left to stir for 1 hour, centrifuged, the supernatant was removed and the solution resuspended in PBS. The NLS used here consists of the following amino acid sequence: GPKKKRKVGGC. An excess of NLS was used to assure the maximum coverage of the entire surface of the sulfo-SMCC-GNR. GNR Functionalization with sulfo-SMCC and NLS was performed on the day of the experiment.

Figure 4.1a shows a Transmission Electron Microscope (TEM, JEOL JEM 1010) image of a sample of GNRs. The size of the GNRs is about 53 ($\pm$ 6) x 20 ($\pm$ 5) nm. GNRs were covered with a PEG layer, not visible in the TEM image. The size of PEG was previously estimated to be about 8 nm (Chapter 2, Supplementary Figure S1). A schematic depiction of the GNR functionalization is shown in Fig. 4.1b-d. PEG-GNRs functionalized with sulfo-SMCC but not with NLS were used as control. The successful functionalization of the GNRs with NLS was confirmed by the UV-Vis spectrum of the GNRs (Suppl. Fig. S1a). To show that the NLS was functional in HeLa cells, we injected NLS-carboxyl-fluorescein in HeLa cells and observed translocation to the nucleus, which did not occur injecting the dye only (Suppl. Fig. S1b, c).

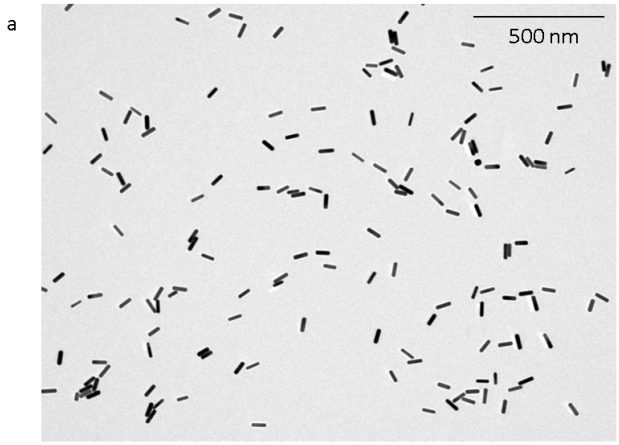

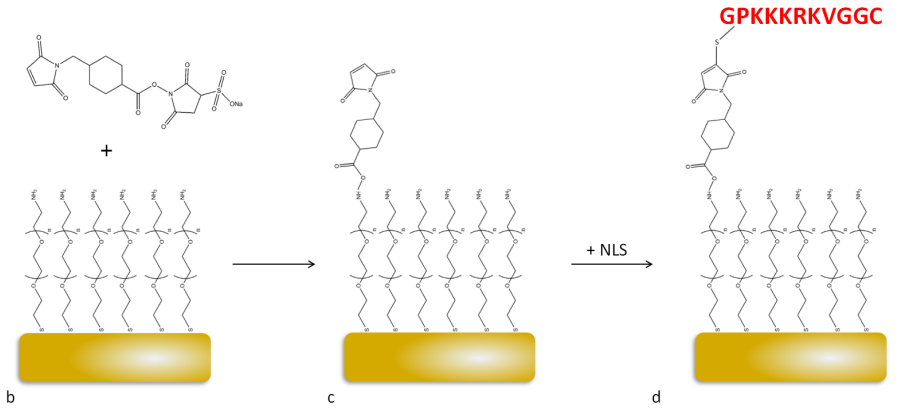

Figure 4.1
GNRs functionalization. a) TEM image of GNRs. b) PEG-GNR and a sulfo-SMCC molecule. c) A PEG-GNR functionalized with sulfo-SMCC-GNR. d) Functionalization of the PEG-GNR-sulfo-SMCC with NLS. The schemes are not in scale.

Cell culture and single-cell microinjection

On the day prior to injection, HeLa cells were plated in Dulbecco's modified eagle's medium (DMEM, Gibco) containing fetal calf serum (FCS) and kept at at 37 °C and 5% CO_2. Cells were incubated with Hoechst (3442, Thermofisher) for 20 minutes for nuclear staining, and subsequently washed 3 times and kept in DMEM. The injection was carried out as described in Chapter 3, Section 3.2.

Imaging

For confocal imaging, cells were imaged 20 minutes after injection on a Leica SPE microscope using a 63x objective (Leica) and a 488 nm laser.

A home-made two-photon multifocal scanning microscope [14] was used for two-photon imaging. The excitation beam, generated with a pulsed IR laser (Chameleon Ultra, Coherent), was split into an array of 25x25 focal spots by a diffractive optical element (custom-made by Holoeye Photonics). The array of beams was then scanned by a scanning mirror (FSM-300, Newport). A square wide-field illumination was thus obtained, covering an area in the sample of approximately 60 μm x 60

μm. A piezo-actuator (P-726 Pifoc, PI) was used to move the objective (60x APOTIRF, Nikon) in the z direction to acquire frames at different z positions. A LED light was used to obtain transmission images of the cells. More details on the setup can be found in Chapter 1, Section 1.2.3.

We acquired 3D movies of GNRs in cells, alternating 3D stacks of fluorescent images with transmission images of the cells. A fluorescent stack was made of typically 15 to 20 2D frames, spaced 0.5 μm between each other. The acquisition rate was 8 frames/s. Fluorescent images were acquired with a wavelength of 770 nm, exciting both GNRs and Hoechst. When the Hoechst intensity was too high to clearly distinguish GNRs, a long-pass filter at 515 nm was used to partially filter the dye.

Localization of GNRs inside cells

We distinguished the GNRs in the cytoplasm, in the nucleus and in the nuclear membrane using the 3D images of each cell. The peaks not overlapping with the Hoechst staining were counted as residing in the cytoplasm. GNRs on the edges of the Hoechst staining were counted as membrane-bound, while GNRs inside the regions labeled by Hoechst staining were counted as localized in the nucleus. It was not possible to distinguish between GNRs on the external or internal side of the nuclear membrane.

Mobility analysis

In every 3D stack of images the position of individual peaks was obtained by fitting with a 3D Gaussian function. The coordinates of GNRs in different 3D stacks were connected to obtain time trajectories. Traces shorter than 4 frames (about 8 seconds) were excluded from the analysis. In each movie we defined the regions corresponding to cell nuclei using the Hoechst staining. We analyzed the mobility of GNRs in the cytoplasm, both for NLS-GNRs and sulfo-SMCC-GNRs. We did not analyze the mobility of GNRs in the nucleus and nuclear membrane due to the difficulty to automatically distinguish between these populations. In few cases, GNRs were present outside the cells: we did not consider these in the analysis.

To analyze the mobility of the particles, we calculated the mean squared displacement (MSD), as described in Chapter 2 and 3. The MSD of a trajectory for a time step τ is the average of the squared

displacements covered by the particle in all steps with a delay of τ. In the case of a freely diffusing particle, the MSD exhibits a linear dependence on τ, that defines the diffusion coefficient D of the particle:

$$MSD(\tau) = 6\sigma^2 + 6D\tau \tag{4.1}$$

From fitting the MSD we obtain the diffusion coefficient D. The localization accuracy σ was for every single GNR fixed to the value based on its photon emission, as described in Chapter 2.

To identify immobile GNRs we used a threshold based on the localization accuracy of the setup. Based on the typical photon emission of the GNRs we use for our experiments, the localization accuracy in 3D is approximately 40 nm. GNRs showing a MSD at any time point lower than 6 times the square of the localization accuracy (0.0096 μm^2) were considered immobile.

The presence of a confinement limiting the particle mobility results in a negative curvature in the MSD that depends on the confinement radius R (Chapter 3, Eq. 3.3). If an active component is present in the motion, a positive curvature will be introduced, that depends on the velocity of the particle (Chapter 3, Eq. 3.2). However, using the current measurement parameters, it was not possible to accurately obtain R or v from individual traces. The movies were acquired for typically 2 to 3 minutes, and GNRs traces were typically less than 10 points long. As anticipated in Chapters 2 and 3, the error on each MSD point is strongly influenced by the length of the trajectory. Therefore, it was not possible to distinguish a curvature in MSD plots from stochastic variations of a single trace and to reliably determine the mobility mode (free diffusion or confined diffusion) from the curvature. Instead, we analyzed the ensemble distribution of MSD values at each time step to distinguish populations with different mobility modes by thresholding the MSD at the largest τ. We then fitted the MSD plot of individual traces with the corresponding mode and quantified the mobility parameters. This approach is the same we used in Chapter 3. Unfortunately, it does not allow to distinguish active populations.

The MSD analysis of GNRs traces was performed in LabVIEW. To assess the significance of differences in results between GNRs from different samples we used a Single-Factor Analysis of Variance (ANOVA), with a p-value threshold of 0.05. For non-Gaussian distributions, a non-

parametric ANOVA (Kruskal-Wallis tes) was used.

4.3 Results

4.3.1 Reproducibility of single-cell microinjection

We characterized the reproducibility of the injection yield, comparing experiments carried out under the same conditions. Within each experiment, we injected NLS-GNRs and sulfo-SMCC-GNRs (used as control) in separate cell samples coming from the same culture. NLS-GNRs and sulfo-SMCC-GNRs originated from the same GNR batch. The experiment was repeated at least 4 times. The number of injected GNRs per cell showed significant differences between NLS-GNRs and sulfo-SMCC-GNRs within a single experiment (Fig. 4.2a,b). In some cases the number of injected sulfo-SMCC-GNRs was significantly lower than the number of NLS-GNRs. Also the number of cells containing GNRs (positive cells) was larger in NLS experiments than in control experiments (Suppl. Fig. S2a,b). Interestingly, for NLS-GNRs, the number of positive cells appeared to increase after 1 hour, while for sulfo-SMCC-GNRs this number decreased. The variation of total number of GNRs per experiment is shown in Suppl. Fig. S2c,d. Some differences in the GNRs samples might be attributed to different properties of the GNR samples. The UV-Vis spectra of the solutions (Supplementary Fig. S2e,f) feature a red-shift of the sample used in the first experiment, compared to the sample used for the later experiments. In addition, the size of the GNRs increased from 53 $\pm$ 6 nm x 20 $\pm$ 5 nm to approximately 60 $\pm$ 6 nm x 23 $\pm$ 5 nm. Though, it is not straightforward to relate these properties to injection yield.

We checked whether the presence of more NLS-GNRs in the nucleus as compared to sulfo-SMCC-GNRs was due to the larger number of NLS-GNRs in cells. The correlation between the number of NLS-GNRs localized in the nucleus and the total number of NLS-GNRs per cell is plotted in Fig. 4.2c. The plots, split up per experiment, are in Supplementary Fig. S2 g-j. Experiment 1 shows the most successful translocation of NLS-GNRs in the nucleus and a clear correlation between the total number of NLS-GNRs in the cell and the number of NLS-GNRs in the nucleus, but nuclear localization is not always found in cells with the highest number of GNRs. The microinjection yield of the other experiments is much smaller, precluding a proper analysis due

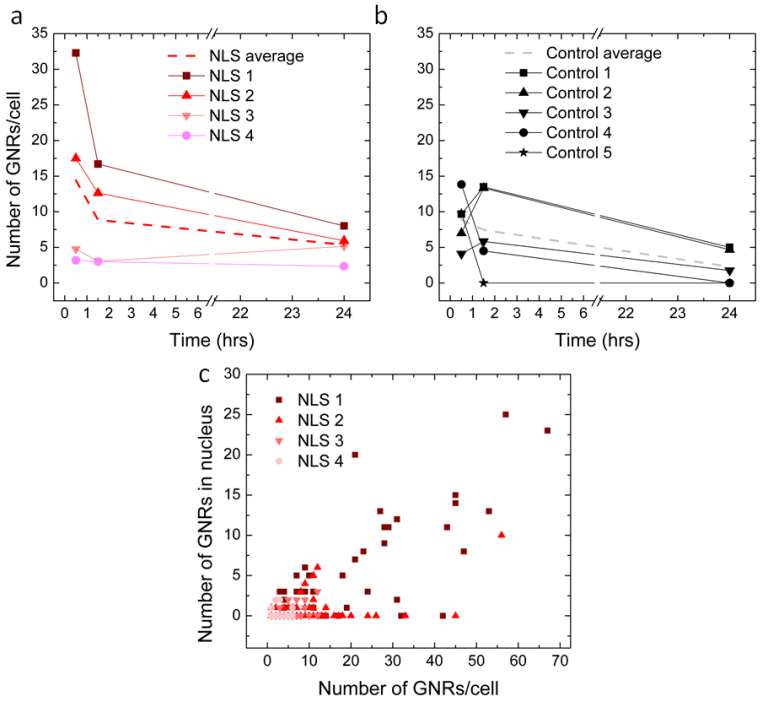

Figure 4.2
The injection efficiency varies between experiments. Variations in the number of GNRs injected per cell between different a) NLS experiments and b) control experiments. c) Number of NLS-GNRs found in the nucleus as a function of the total number of NLS-GNRs per cell among the 4 NLS experiments.

to the small number of GNRs. In the following, we either pooled all experiments or analyzed one experiment in detail, to recover details of the faith of GNRs in cells.

4.3.2 Localization of functionalized gold nanorods inside cells

Figure 4.3 shows some representative images of cells injected with NLS-GNRs (4.3a-c) and sulfo-SMCC-GNRs (4.3d-f). To localize GNRs in the nucleus or on the membrane, the 3D movie was used. We imaged the cells at three time points after injection: 0.5, 1.5 and 24 hours. The Hoechst staining indicates the cell nuclei, but gets weaker over time due to bleach-

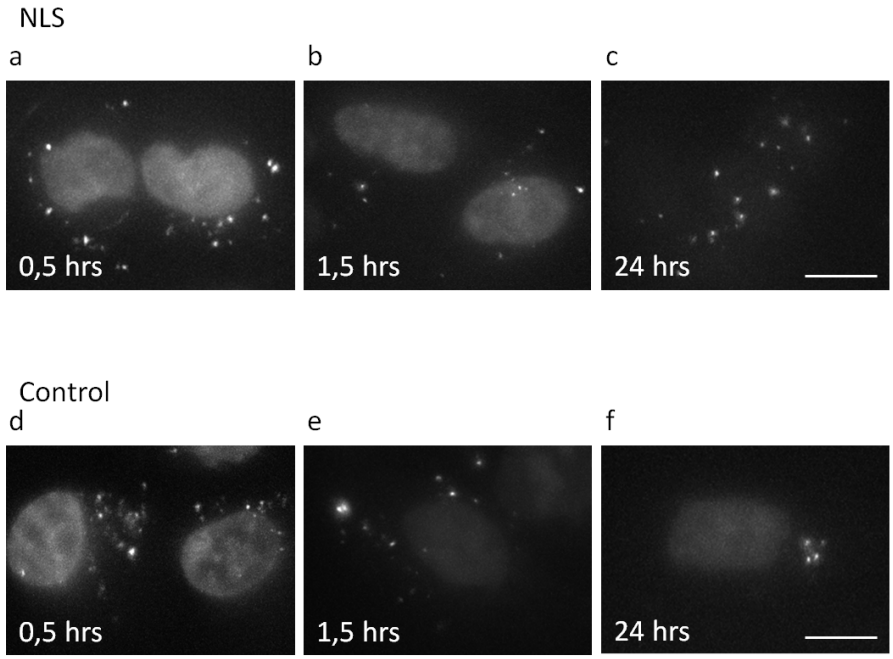

Figure 4.3
Two-photon images of HeLa cells injected with NLS-GNRs and sulfo-SMCC-GNRs, imaged at different time points after injection. a-c) Cells with NLS-GNRs, d-f) cells with Sulfo-SSMC-GNRs. Images at 0.5, 1.5 and 24 hours post injection are shown. Cell nuclei were stained with Hoechst. The scale bars correspond to 10 μm.

ing. NLS-GNRs were found in the cytoplasm, around the nuclear membrane and in the nucleus of cells. In contrast, sulfo-SMCC-GNRs were only found in the cytoplasm or around the nuclear membrane, with few exceptions. Even though not all cells showed healthy morphology after injection, injected cells with good viability, as judged by their shape, were found till up to 120 hours after injection in the case of NLS-GNRs (Supplementary Figure S3a) and up to 48 hours in the case of sulfo-SMCC-GNRs (Supplementary Figure S3b), well beyond the duration of our experiment.

We quantified the number of GNRs in the nucleus, nuclear membrane and cytoplasm of cells over time, pooling all experiments, and

compared the results for NLS-GNRs and sulfo-SMCC-GNRs, which was used as control. The results are shown in Figure 4.4. We found an average of 2 NLS-GNRs in the nucleus at all three time points (Figure 4.4a), though the variation in the number of nuclear NLS-GNRs was very large (up to about 30 GNRs in experiment 1). We only observed a few nuclear sulfo-SMCC-GNRs: the difference with the number of nuclear NLS-GNRs is statistically significant. Note that the 3D stack of images is necessary to distinguish GNRs in the nucleus or bound to the nuclear membrane: for this reason, some GNRs that seem to localize in the nucleus in a projected image (see example in Fig. 4.3d,e) are instead membrane-bound. Both NLS-GNRs and sulfo-SMCC-GNRs were found in or around the nuclear membrane (Figure 4.4b). An average of 5 NLS-GNRs and 3 sulfo-SMCC-GNRs were in the membrane at 0.5 hours post injection; both numbers decreased over time, but no significant difference was found between NLS-GNRs and sulfo-SMCC-GNRs in this compartment. In the cytoplasm, (Figure 4.4c) we counted an average of 7 NLS-GNRs and 5 sulfo-SMCC-GNRs at 0.5 hours post injection, both decreasing significantly over time. No significant difference was observed between NLS-GNRs and sulfo-SMCC-GNRs in the cytoplasm. The details of the distribution of GNRs in each compartment in time can be found in Supplementary Fig. S4a-c.

Overall, the percentage of GNRs translocating to the nucleus is about 15% when functionalized with NLS and less than 2% for sulfo-SMCC-GNRs (Fig. 4.4d). This result demonstrates successful targeting of GNRs in the nucleus, albeit with relatively low yield. Note that the percentage of nuclear NLS-GNRs at 24 hours after injection increases due to the loss of GNRs in the cytoplasm. The increase in percentage of sulfo-SMCC-GNRs in the membrane is due to the same reason.

4.3.3 Mobility of functionalized gold nanorods

We analyzed the mobility of NLS-GNRs and sulfo-SMCC-GNR in the cytoplasm of injected cells. Visual inspection of the MSD histograms suggests the presence of two populations both in NLS-GNRs and sulfo-SMCC-GNRs (Supplementary Figure S5). A population with MSD lower than 0.2 μm^2 is stable in time, consistent with confined GNRs, while MSDs larger than 0.2 μm^2 increase over time, typical for free diffusion. In addition to mobile GNRs, an immobile fraction was found with a constant MSD that does not exceed the positional accuracy. Though we

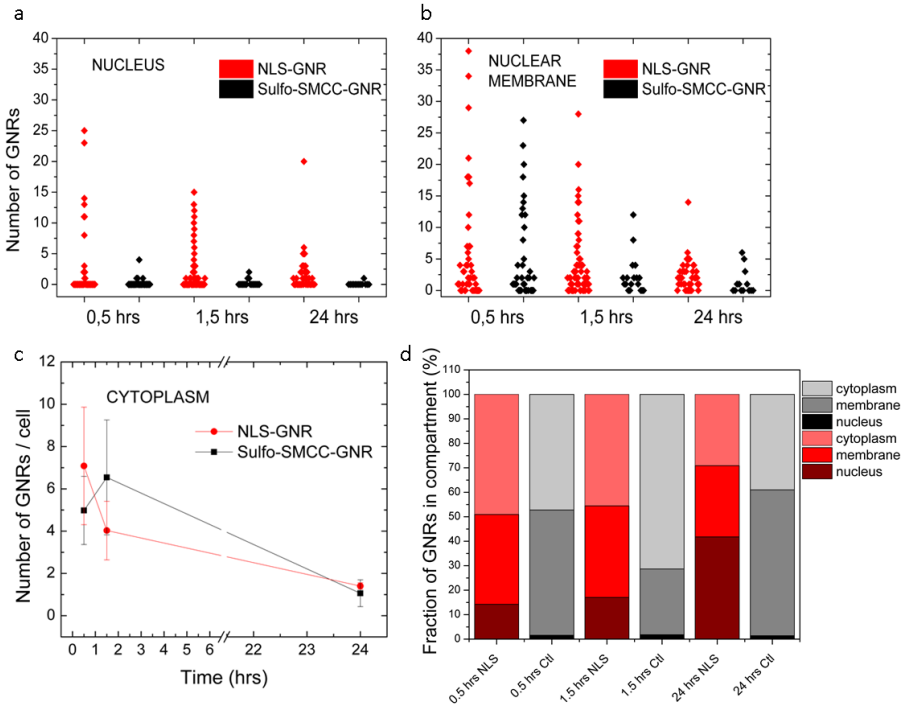

Figure 4.4

Difference in the distribution of NLS-GNRs and sulfo-SMCC-GNRs in cells over time. a) Number of GNRs in the nucleus over time, in NLS (red) and control experiment (black). b) Number of GNRs in the nuclear membrane over time. c) Number of GNRs in the cytoplasm over time. The numbers are the mean and standard deviation in 5 control and 4 NLS experiments. d) Bar plot of percentages of GNRs in each compartment over time, in NLS (NLS-GNRs) and control experiments (sulfo-SMCC-GNRs).

observed some variations, it appears that the MSD of the GNRs does not change with time after injection.

Next, we fitted the MSD of single traces to obtain the diffusion coefficients or the confinement sizes. For the traces that were assigned to be confined, we observed a constant MSD that exceeded the positional accuracy. This implies a D that is faster than can be resolved given the time resolution of our experiment. Therefore we only fitted the confinement sizes in these cases. Table 4.1 reports the mobility results. The number of immobile GNRs and the corresponding percentage of the total number of traces is shown for the immobile fraction. The number of traces in each population and the corresponding percentage, the median, 1^{st} and 3^{rd} quartiles of the diffusion coefficients and confinement sizes are reported for mobile GNRs. Note that all the distributions exhibited a longer tail of large values, thus they deviate from normal distributions (see histograms in Supplementary Fig. S6). The distributions of diffusion coefficients and confinement sizes are shown in the box plots in Fig. 4.5a,b. No significant difference was found among the parameters at different time points for both NLS-GNRs and sulfo-SMCC-GNRs (Supplementary Figure S7 and Supplementary Tables S2 and S3), so we pooled the results from all time points.

The percentages relative to each population are summarized in Fig. 4.5c. The detailed percentages relative to each time point are reported in Supplementary Fig. S8. The immobile population amounts to 17% in NLS-GNRs and 9% in sulfo-SMCC-GNRs. The confined population is about 46% of the total number of NLS-GNRs and 53% of the population of sulfo-SMCC-GNRs. The median of the confinement radius is 0.4 μm both in cells injected with NLS-GNRs and sulfo-SMCC-GNRs. The distribution of confinement radii is larger for NLS-GNRs (Fig. 4.5b), but the difference is not statistically significant. The freely diffusing population is 37% of the NLS-GNRs and 38% of the NLS-GNRs. The median of the diffusion coefficients is 0.005 $\mu m^2/s$ in both cases: this value is compatible with the diffusion coefficients of GNRs freely diffusing in cells we obtained previously (see Chapter 3, Section 3.3.2), as shown in Supplementary Fig. S9. Mobility values of PEG-GNR without functionalization, sulfo-SMCC-GNRs and NLS-GNRs do not show any significant difference (see Supplementary Table S4).

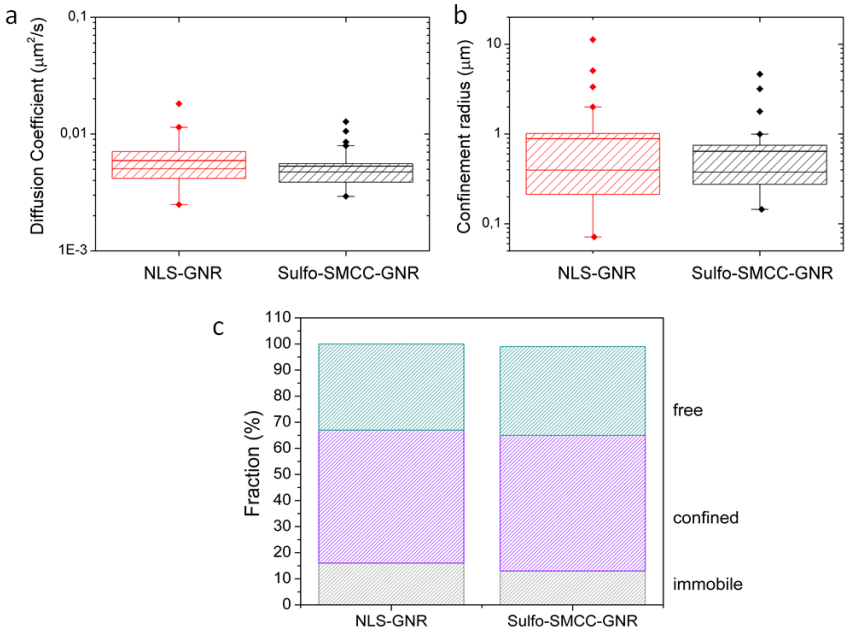

Figure 4.5
Mobility of NLS-GNRs and sulfo-SMCC-GNRs in the cytoplasm. a) Distribution of diffusion coefficients of freely diffusing NLS-GNRs and sulfo-SMCC-GNRs. b) Distribution of the confinement radii for the NLS-GNRs and sulfo-SMCC-GNRs with confined mobility. c) Percentages relative to each GNR population (immobile, freely diffusing and confined) for NLS-GNRs and sulfo-SMCC-GNRs.

4.4 Discussion and conclusion

We used single-cell microinjection to deliver gold nanorods in the cytoplasm of HeLa cells. We tested the fate of gold nanorods functionalized with nuclear localization signal peptides, that induce nuclear targeting. The results were compared with results obtained from gold nanorods not functionalized with the peptides. First, we characterized the reproducibility of the injection procedure, by analyzing differences in outcome between individual repeated experiments. We observed a large variability both in the number of positive cells and in the number of NLS-GNRs and sulfo-SMCC-GNRs injected in cells. We attributed the differences to the composition of the GNRs samples. For GNRs samples that exhibited

Population	Parameter	NLS-GNR	sulfo-SMCC-GNR
Immobile	Pop. Size	25. 17%	7; 9%
Confined	Pop. Size	66; 46%	39; 53%
	Confinement (μm)	0.4 (0.2-1)	0.4 (0.3-0.7)
Freely Diffusing	Pop. Size	53; 37%	28; 38%
	D ($\mu m^2/s$)	0.005 (0.004-0.007)	0.005 (0.004-0.006)

Table 4.1
Mobility parameters obtained for NLS-GNRs and sulfo-SMCC-GNRs. The table reports the number of traces corresponding to each population and the relative percentages. For the confined populations, the median, 1^{st} and 3^{rd} quartiles of the confinement sizes are reported. For the freely diffusing populations, the median, 1^{st} and 3^{rd} quartiles of the diffusion coefficients are reported.

a blue-shift, the excitation was less efficient at 770 nm wavelength, and might explain the reduced number of GNRs we see in later experiments. The blue-shift can be due to the growth of particles in the samples over time after synthesis, due to the presence of free gold in the growth solution that was not properly removed. TEM images of the samples used for the last experiments showed indeed an increased particle size.

The number of positive cells varied between the NLS and control experiments, but also within the same experiments over time. Cases of reduction in the number of positive cells over time can be due to cell death, while cases of increase of positive cells can be explained in two ways. Cells may release some GNRs, which could subsequently be taken up by other cells (as also hypothesized in [13]). Alternatively, we could have missed positive cells at some time point, due to the difficulty in finding the injected cells not in close proximity to the marker in the sample. For control experiments the low number of positive cells at 24 hours can result from a loss of sulfo-SMCC-GNRs in the cytoplasm. However, given the small number of cells, due to the relatively low throughput of the microinjection technique, and the large number of parameters that could affect injection efficiency and the fate of GNRs, it is at this point not possible to substantiate such scenarios.

Due to the difficulty in obtaining the same conditions in individual experiments, the results from different individual experiments exhibited some variations. Nevertheless, in all experiments we observed translocation of NLS-GNRs to the nucleus of HeLa cells. The translocation efficiency was variable between different experiments, yet generally low. Adding all individual experiments, the absolute number of NLS-GNRs localized in the nucleus is low (2 on average). In percentage, this corresponds to an efficiency of about 15%. This value is significantly different from the percentage of sulfo-SMCC-GNRs found in the nucleus, that is less than 2%. The large size of the GNRs (from approximately 53 nm x 20 nm to 60 nm x 23 nm, plus a PEG layer of about 8 nm) might explain the low efficiency of nuclear delivery. Some NLS-GNRs were found in the nuclear membrane: this could be due to the impossibility of entering the nucleus when the GNRs are too large. It is possible that only GNRs with a favorable orientation (perpendicular to the surface of the membrane) could enter the nuclear pores. However, there is no significant difference with the number of sulfo-SMCC-GNRs located around the membrane. We tested smaller GNRs but these proved a higher stickiness that affected severly the delivery efficiency by microinjection (data not shown).

Previously, successful nuclear targeting was reported for particles with sizes up to 40 nm [17], mostly using nanospheres [9, 11, 12]. Oyelere et al [8] reported successful nuclear translocation of GNRs functionalized with NLS and delivered in cells through incubation. However, these GNRs were smaller than the ones we used (about 40 nm x 15 nm) and not PEGylated (the PEG layer increases the final size of the particles of about 8 nm for each side). In addition, 2D images were used to assess the location of the GNRs, it was therefore hard to distinguish GNRs in the nucleus or bound to the nuclear membrane. The translocation into the nucleus of NLS-GNRs that we observed occurred within the first half an hour, in agreement with previous findings [17].

The number of GNRs in the cytoplasm showed no difference between NLS and control experiments, and in both cases this number decreased in time. As there was no significant change over time in the number of GNRs in the nucleus and in the nuclear membrane, the decreasing number of particles in the cytoplasm cannot be due to translocation to the other compartments. The loss of GNRs in the cytoplasm might be due to exocytosis. Exocytosis of particles localized in the cytoplasm was

observed previously [13, 18]. The impossibility for particles larger than 10 nm to cross the nuclear membrane in absence of a specialized localization signal (the NLS works only to signal towards the nucleus and not back [4]), explains the absence of exocytosis of nuclear GNRs. GNRs localized on the external surface of the nuclear membrane might be stuck, therefore they cannot be excreted.

We analyzed the mobility of the GNRs in the cytoplasm of the injected cells. We found an immobile population, equal to 17% of the NLS-GNRs and 9% of the sulfo-SMCC-GNRs. These results are obtained pooling all time points, and their difference is mainly due to the absence of immobile sulfo-SMCC-GNRs at 24 hours, a result probably related to the loss of particles that resided in the cytoplasm. The presence of a significant fraction of immobile GNRs is compatible with our previous results obtained with non-functionalized GNRs (Chapter 3), and might be explained by sticking of GNRs to immobile structures in the cells, like organelles or filaments [19].

The fraction of freely diffusing GNRs is comparable in NLS and control experiments (46% and 53%). The diffusion coefficient we obtained has in both cases a median value of 0.005 $\mu m^2/s$. This value is about 3 orders of magnitude lower than the expected ones for GNRs of similar size in cells, and it is comparable to our previous findings (see Chapter 3, [14]), in which we observed the same diffusion coefficients both in cytoplasm and nucleus of HeLa cells: hence it cannot be due to internalization into vesicles. We instead hypothesized a reduction in the diffusion due to the presence of obstacles in cell and the stickiness of the PEG-GNRs. This explanation may also be valid for the results presented here for nanorods functionalized with sulfo-SMCC and NLS.

A third population of GNRs shows a motion limited by spatial confinement. This could be explained by internalization of GNRs into vesicles, or by hindered diffusion due to obstacles encountered in the cytoplasm [20]. The range of confinement sizes we obtain is compatible with typical sizes of organelles or free spaces in the cytoplasm. Some large outliers (less than 10%) with confinement sizes from 1 to 10 μm are present. We attribute these outliers to free particles with a MSD lower than 0,2 μm^2, that can hardly be distinguished from confined GNRs.

The study of the fate of functionalized GNRs would benefit from the

possibility to follow the same individual cells over a longer time. Longer traces could then be acquired, allowing for more precise MSD analysis and making it possible to determine the mobility mode of each individual GNR. To follow the same cells over time it is necessary to incorporate an incubator on the two-photon microscope, in order to maintain the cells in the proper growing conditions during the experiments.

The successful translocation of NLS-GNRs is important for the use of GNRs as labels to follow the dynamics of proteins in live cells. In addition, the use of GNRs for targeted-drug delivery and cytotoxicity studies can benefit from better knowledge about translocation into the nucleus.

4.5 Supplementary figures

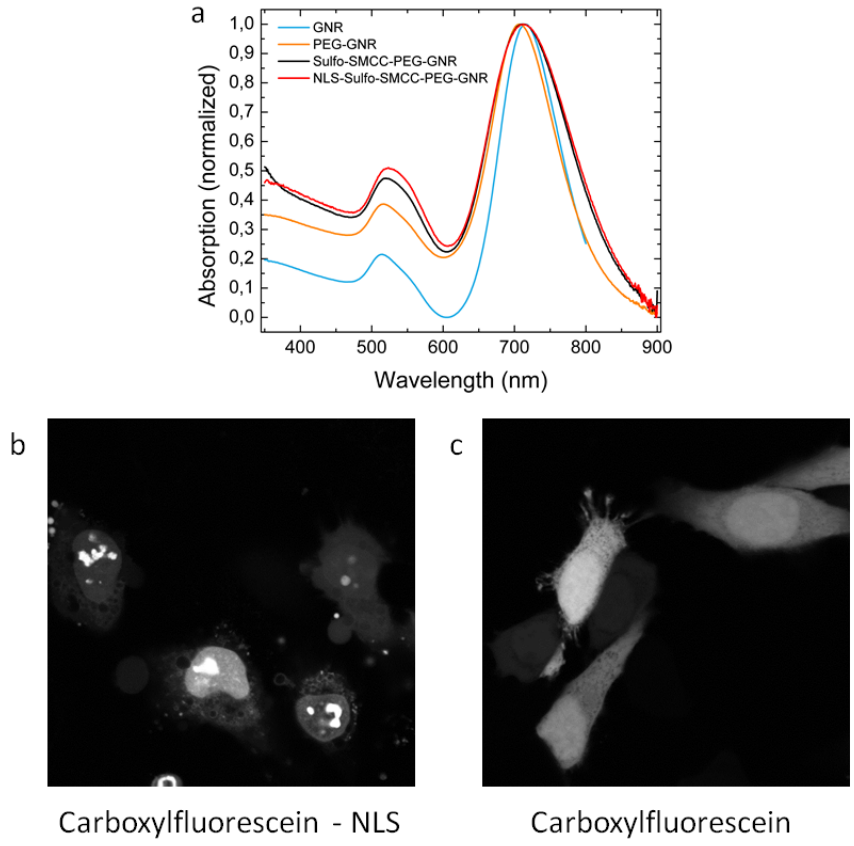

Figure S1
Confirmation of the functionalization of GNRs with sulfo-SMCC and NLS. a) The UV-Vis spectrum of the GNR solution broadens after PEGylation and functionalization with sulfo-SMCC and NLS. Confocal microscope images of HeLa cells injected with b) carboxylfluorescein-NLS and c) only carboxyl-fluroescein show that the NLS peptide induces nuclear translocation, which is absent when only the dye is injected.

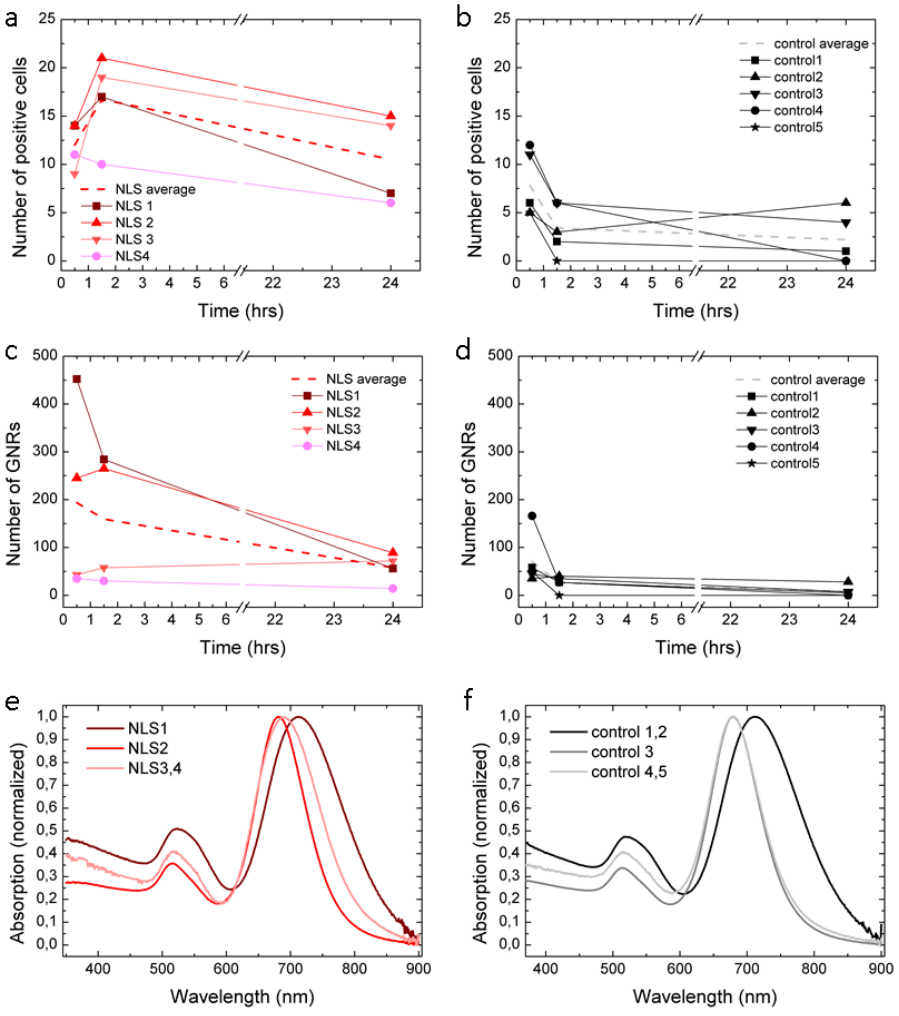
a
Number of positive cells
Time (hrs)
NLS average
NLS 1
NLS 2
NLS 3
NLS4
b
Number of positive cells
Time (hrs)
control average
control1
control2
control3
control4
control5
c
Number of GNRs
Time (hrs)
NLS average
NLS1
NLS2
NLS3
NLS4
d
Number of GNRs
Time (hrs)
control average
control1
control2
control3
control4
control5
e
Absorption (normalized)
Wavelength (nm)
NLS1
NLS2
NLS3,4
f
Absorption (normalized)
Wavelength (nm)
control 1,2
control 3
control 4,5

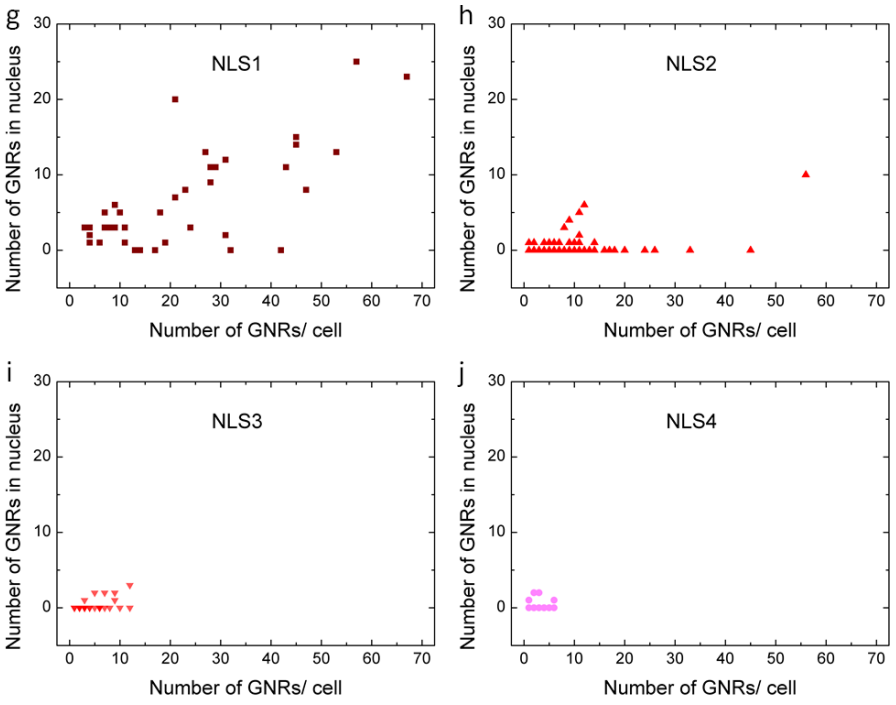

Figure S2

Reproducibility of the injection technique. Number of cells containing GNRs (positive cells) found during a) NLS experiments and b) control experiments. Total number of GNRs found in cells during c) NLS and d) control experiments. UV-Vis spectra of the GNR solutions after functionalization with e) sulfo-SMCC-NLS and f) only sulfo-SMCC. A blue-shift is verified between the sample used for the first and the last experiments. g-j) Number of NLS-GNRs found in cells nuclei in each NLS experiment.

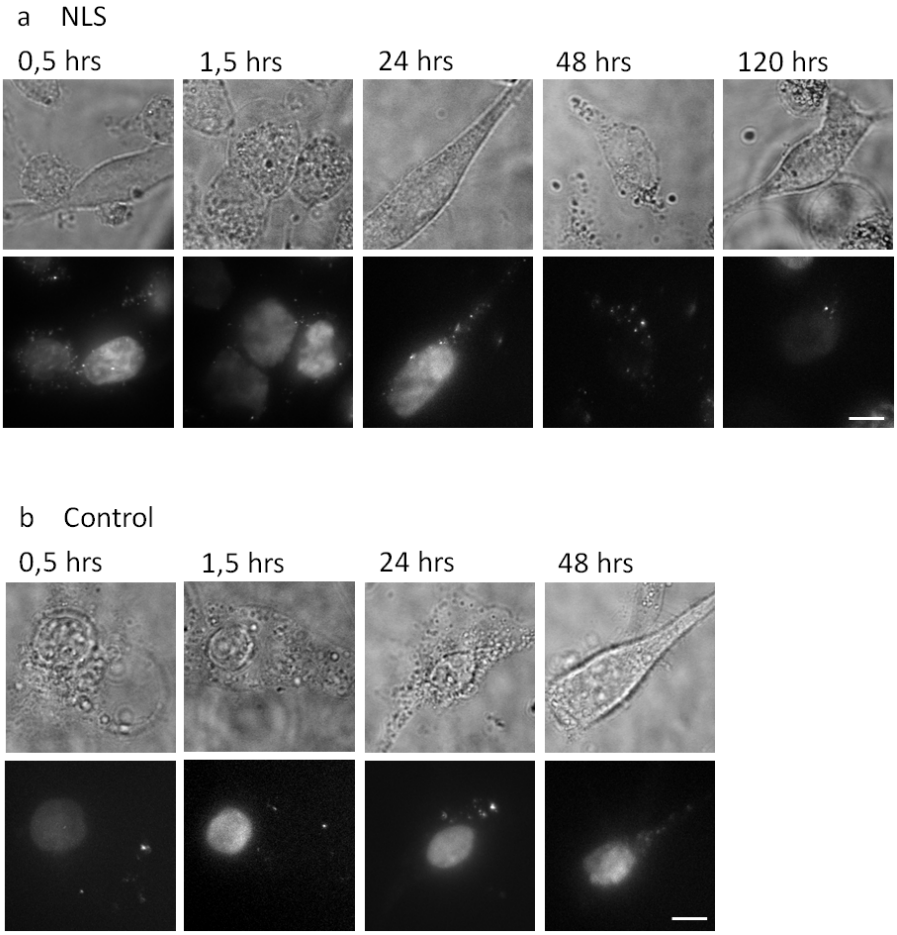

Figure S3

There are variations in the viability of injected cells, however cells with good viability can be found till up to 120 hours after injection with GNRs. Time sequence of transmission and two-photon luminescence images of cells injected with a) NLS-GNRs and b) sulfo-SMCC-GNRs. The size bars are 10 μm.

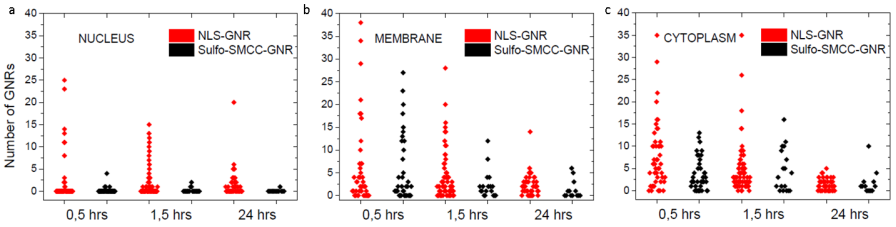

Figure S4

Difference in the distribution of the number of NLS-GNRs and sulfo-SMCC-GNRs per cell over time in each compartment at three time points after injection: in a) nucleus, b) nuclear membrane and c) cytoplasm.

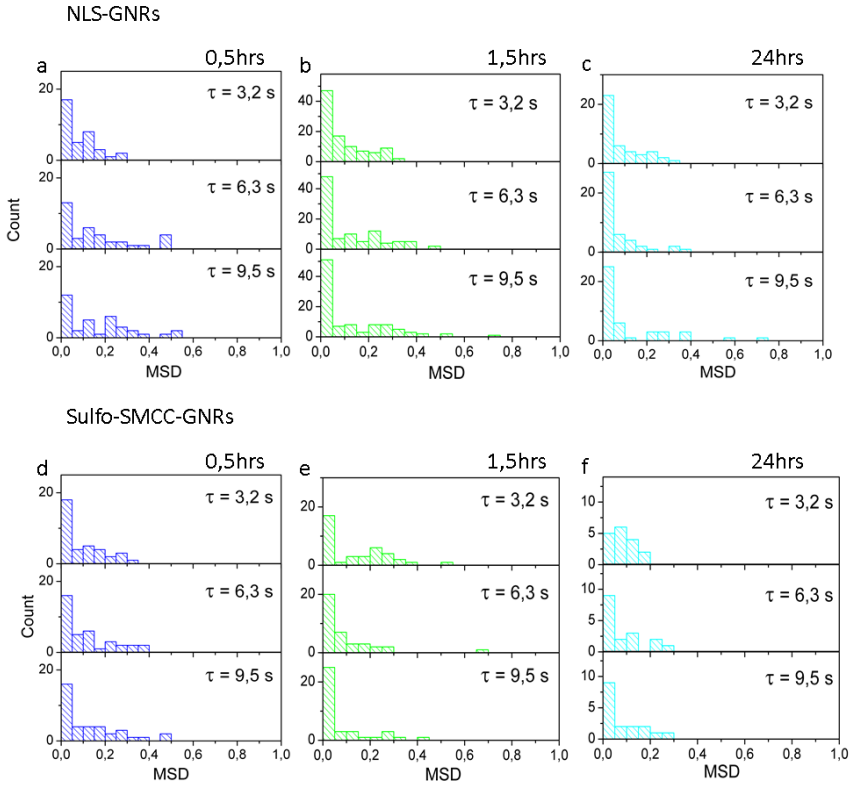

Figure S5

MSD histograms of a-c) NLS-GNRs traces and d-f) sulfo-SMCC-GNRs traces, divided by time after injection.

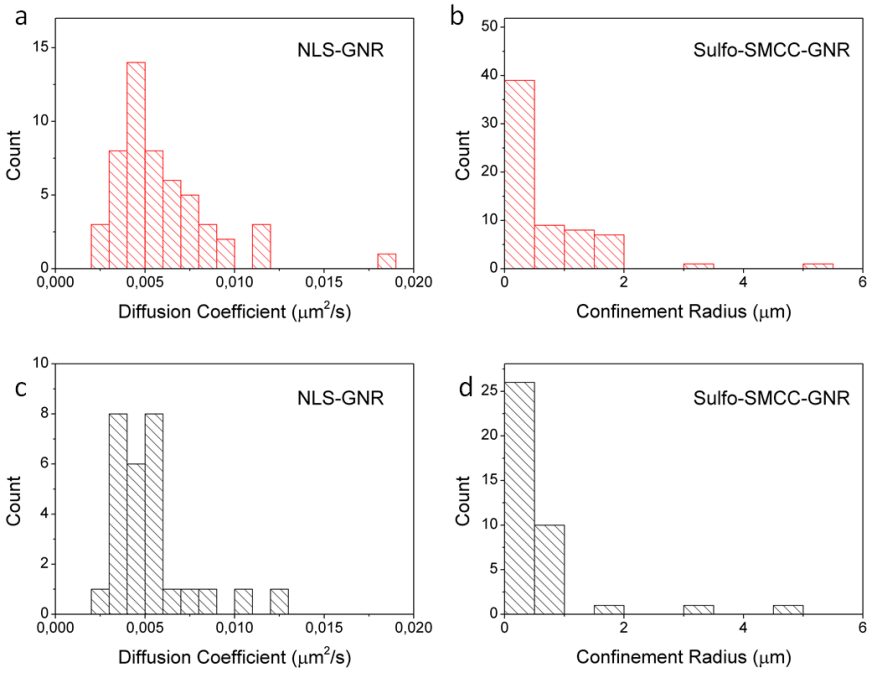

Figure S6

Histograms of diffusion coefficients and confinement sizes for a,b) NLS-GNRs and c,d) sulfo-SMCC-GNRs.

Population	Parameter	NLS-GNR		
	Time post injection (hrs)	0.5	1.5	24
Immobile	Pop. Size	6; 17%	13; 18%	8; 18%
Confined	Pop. Size	15; 45%	28; 41%	23; 52%
	Confinement (μm)	0.4 (0.2-1.2)	0.4 (0.2-1.2)	0.4 (0.2-1)
Freely Diffusing	Pop. Size	12; 38%	28; 41%	13; 30%
	D ($\mu m^2/s$)	0.005 (0.005-0.007)	0.005 (0.004-0.007)	0.006 (0.004-0007)

Table S2

Mobility parameters obtained from NLS-GNRs at three different time points after injection. The number of traces corresponding to each population and the relative percentages are reported. The table reports the median, 1^{st} and 3^{rd} quartile of the confinement size of the confined populations, and the median, 1^{st} and 3^{rd} quartile of the diffusion coefficients of the freely diffusing populations.

Population	Parameter	sulfo-SMCC-GNR		
	Time post injection (hrs)	0.5	1.5	24
Immobile	Pop. Size	4; 18%	6; 18%	0
Confined	Pop. Size	11; 50%	14; 41%	10; 67%
	Confinement (μm)	0.3 (0.2-0.5)	0.7 (0.4-0.8)	0.4 (0.2-0.8)
Freely Diffusing	Pop. Size	7; 32%	14; 41%	5; 33%
	D ($\mu m^2/s$)	0.005 (0.004-0.006)	0.005 (0.004-0.006)	0.005 (0.004-0005)

Table S3

Mobility parameters obtained from sulfo-SMCC-GNRs at three different time points after injection. The number of traces corresponding to each population and the relative percentages are reported. The table reports the median, 1^{st} and 3^{rd} quartile of the confinement size of the confined populations, and the median, 1^{st} and 3^{rd} quartile of the diffusion coefficients of the freely diffusing populations.

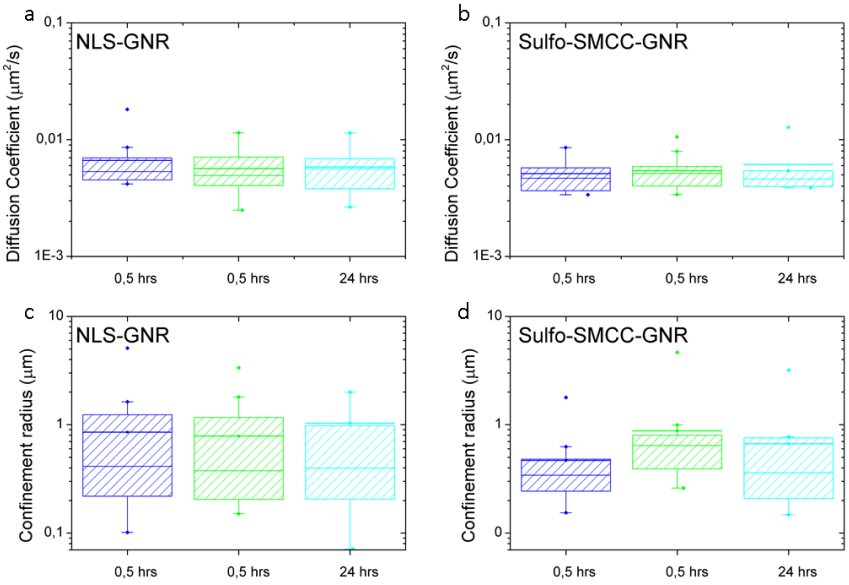

Figure S7
Distribution of diffusion coefficients and confinement radii at each time point after injection, for a,c) NLS-GNRs and b,d) sulfo-SMCC-GNR.

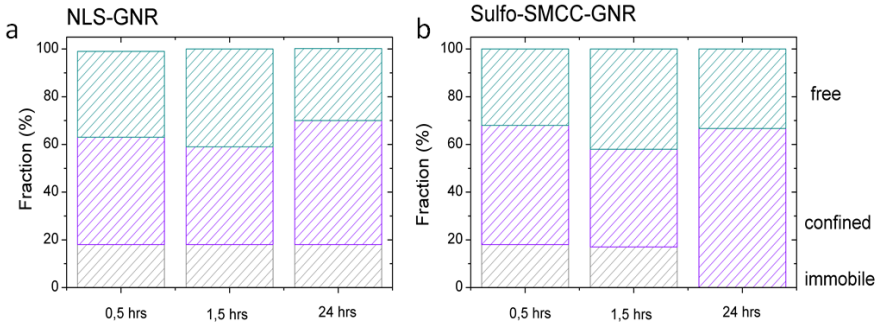

Figure S8
Percentages relative to each GNR population (immobile, freely diffusing of confined) for a) NLS-GNRs and b) sulfo-SMCC-GNRs, divided by time after injection.

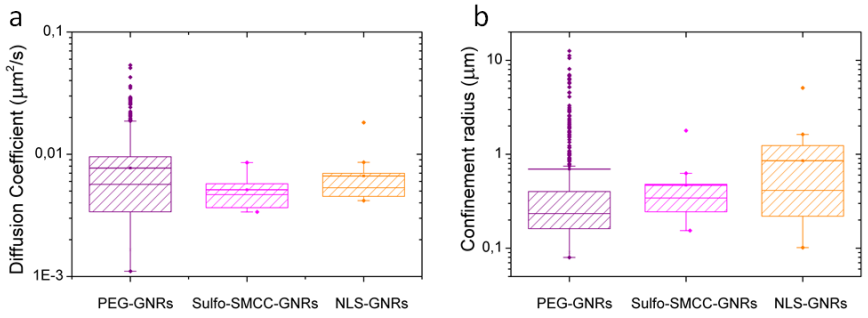

Figure S9

Influence of the functionalization on GNRs mobility. Comparison between the distributions of a) diffusion coefficients and b) confinement radii of PEG-GNRs, PEG-GNRs functionalized with sulfo-SMCC and functionalized with sulfo-SMCC-NLS. The results relative to PEG-GNRs were presented in Chapter 3, Section 3.3.2. In the case of PEG-GNRs, we analyzed the mobility shortly after injection. We compared these results with the ones obtained from sulfo-SMCC-GNRs and NLS-GNRs at 0.5 hours after injection. There are no significant differences in the distributions.

Population	Parameter	PEG-GNR	sulfo-SMCC-GNR	NLS-GNR
Immobile	Pop. Size	125; 13%	4; 18%	6; 18%
Confined	Pop. Size	449; 45%	11; 50%	15; 45%
	Confinement (μm)	0.2 (0.2-0.4)	0.3 (0.2-0.5)	0.4 (0.2-1.2)
Freely Diffusing	Pop. Size	418; 42%	7; 32%	12; 37%
	D ($\mu m^2/s$)	0.006 (0.004-0.009)	0.005 (0.004-0.006)	0.005 (0.004-0007)

Table S4

Mobility parameters obtained from PEG-GNRs, sulfo-SMCC-GNRs and NLS-GNRs, measured 0,5 hours after injection. The table reports the number of traces corresponding to each population and the relative percentages. The median, 1^{st} and 3^{rd} quartile of the confinement sized for the confined populations, and the median, 1^{st} and 3^{rd} quartile of the diffusion coefficients for the freely diffusing populations are reported. The results for PEG-GNRs were presented in Chapter 3, Section 3.3.2.

Bibliography

[1] Ning Zhao et al. "Gold nanoparticles for cancer theranostics: A brief update". In: *Sensors and Actuators B.* (2013).

[2] Mohamed Kodiha et al. "Off to the Organelles: Killing Cancer Cells with Targeted Gold Nanoparticles". In: *Theranostics* 5.4 (2015), pp. 357–370. ISSN: 1838-7640.

[3] Allison Lange et al. "Classical Nuclear Localization Signals: Definition, Function, and Interaction with Importin Alpha". In: *Journal of Biological Chemistry* (2006).

[4] Shuaidong Huo et al. "Ultrasmall Gold Nanoparticles as Carriers for Nucleus-Based Gene Therapy Due to Size-Dependent Nuclear Entry". In: *ACS Nano* 8.6 (June 2014), pp. 5852–5862. ISSN: 1936-0851.

[5] Yan-Juan Gu et al. "Nuclear penetration of surface functionalized gold nanoparticles". In: *Toxicology and Applied Pharmacology* 237.2 (2009), pp. 196–204. ISSN: 0041008X.

[6] Alexander G Tkachenko et al. "Multifunctional gold nanoparticle-peptide complexes for nuclear targeting." In: *Journal of the American Chemical Society* 125.16 (Apr. 2003), pp. 4700–1. ISSN: 0002-7863.

[7] Wei Qian et al. "Dark-field light scattering imaging of living cancer cell component from birth through division using bioconjugated gold nanoprobes". In: *Journal of Biomedical Optics* 15.4 (2010), p. 046025. ISSN: 10833668.

[8] Adegboyega K. Oyelere et al. "Peptide-conjugated gold nanorods for nuclear targeting." In: *Bioconjugate chemistry* 18.5 (2006), pp. 1490–7. ISSN: 1043-1802.

[9] Wei Xie et al. "Nuclear Targeted Nanoprobe for Single Living Cell Detection by Surface-Enhanced Raman Scattering". In: *Bioconjugate Chemistry* 20.4 (Apr. 2009), pp. 768–773. ISSN: 1043-1802.

[10] Paola Nativo, Ian Prior, and Mathias Brust. "Uptake and intracellular fate of surface-modified gold nanoparticles." In: *ACS nano* 2.8 (Aug. 2008), pp. 1639–44. ISSN: 1936-086X.

[11] Bin Kang, Megan Mackey, and Mostafa A. El-Sayed. "Nuclear Targeting of Gold Nanoparticles in Cancer Cells Induces DNA Damage, Causing Cytokinesis Arrest and Apoptosis". In: *Journal of the American Chemical Society* 132.5 (Feb. 2010), pp. 1517–1519. ISSN: 0002-7863.

[12] Megan Mackey and Mostafa El-Sayed. "Chemosensitization of cancer cells via gold nanoparticle-induced cell cycle regulation." In: *Photochemistry and photobiology* 90.2 (2014), pp. 306–12. ISSN: 1751-1097.

[13] C. Yang et al. "Peptide modified gold nanoparticles for improved cellular uptake, nuclear transport, and intracellular retention". In: *Nanoscale* 6.20 (Aug. 2014), pp. 12026–12033. ISSN: 2040-3364.

[14] Bram van den Broek et al. "Parallel nanometric 3D tracking of intracellular gold nanorods using multifocal two-photon microscopy." In: *Nano letters* 13.3 (Mar. 2013), pp. 980–6. ISSN: 1530-6992.

[15] Babak Nikoobakht and Mostafa A. El-Sayed. "Preparation and Growth Mechanism of Gold Nanorods (NRs) Using Seed-Mediated Growth Method". In: *Chemistry of Materials* 15.10 (May 2003), pp. 1957–1962. ISSN: 0897-4756.

[16] Nicolas Bogliotti et al. "Optimizing the formation of biocompatible gold nanorods for cancer research: Functionalization, stabilization and purification". In: *Journal of Colloid and Interface Science* 357.1 (2011), pp. 75–81. ISSN: 00219797.

[17] Nelly Pante and Michael Kann. "Nuclear pore complex is able to transport macromolecules with diameters of about 39 nm." In: *Molecular biology of the cell* 13.2 (Feb. 2002), pp. 425–34. ISSN: 1059-1524.

[18] Zhiqin Chu et al. "Unambiguous observation of shape effects on cellular fate of nanoparticles". In: *Scientific Reports* 4 (Mar. 2014), pp. 3050–3061. ISSN: 2045-2322.

[19] Peter H. Hemmerich et al. "Defining the Subcellular Interface of Nanoparticles by Live-Cell Imaging". In: *PLoS ONE* 8.4 (Apr. 2013). Ed. by Bing Xu, e62018. ISSN: 1932-6203.

[20] Gernot Guigas and Matthias Weiss. "Sampling the Cell with Anomalous Diffusion-The Discovery of Slowness". In: *Biophysical Journal* 94.1 (2008), pp. 90–94. ISSN: 00063495.